Appl. Phys. B 68, 169–175 (1999)

Applied Physics B
Lasers
and Optics

High-peak-power femtosecond Cr:forsterite laser system

T. Togashi, Y. Nabekawa, T. Sekikawa, S. Watanabe

Institute for Solid State Physics, University of Tokyo, 7-22-1 Roppongi, Minato-ku, Tokyo 106-8666, Japan
(Fax: +81-3/3478-4496, E-mail: tadashi@evans.issp.u-tokyo.ac.jp)

Received: 25 June 1998

Abstract. We have developed a high-peak-power Cr:forsterite laser based on a regenerative amplifier. The output energy was 0.4 mJ with a pulse duration of 77 fs at a 10 Hz repetition ratio, resulting in a peak power of 5.2 GW, which as far as we know is the highest power ever obtained from Cr:forsterite laser. To switch the regenerative amplifier rapidly, we developed a Pockels cell driver based on fast high-voltage transistor switches. We also investigated the effects of excited-state absorption on the gain numerically and experimentally. The way to optimize the regenerative amplifier is indicated by the analytical results obtained using a model including absorption in the crystal and excited-state absorption.

PACS: 42.60; 42.55; 42.79

Chromium-doped forsterite (Cr^{4+}:Mg_2SiO_4) was the first near-infrared tunable solid-state laser material that employed Cr^{4+} as an active ion. Since the operation of Cr^{4+}:forsterite lasers was first demonstration several years ago [1–3], the spectroscopic and laser properties of forsterite have been investigated extensively, [4–9] and mode-locked picosecond and femtosecond operation [10–14] has resulted in pulses as short as 20 fs [13]. This material offers a broadband gain near 1.3 μm, a near-infrared wavelength region not accessible by Ti^{3+}:sapphire and Cr^{3+}-based lasers. Furthermore, the second harmonic of a Cr:forsterite laser fills the gap between the fundamental and the second harmonic of a Ti^{3+}:sapphire laser [15].

Recently, high-peak-power, ultrashort pulse laser systems have been developed by using Ti^{3+}:sapphire as a gain medium [16–20]. These systems were made possible by the chirped-pulse amplification (CPA) technique [21], and we have applied this technique to the Cr^{4+}:forsterite laser system. Cr^{4+}:forsterite offers potential advanstages over Ti^{3+}:sapphire with regard to the scaling up of output power. The quantum efficiency (laser wavelength/pump wavelength) is higher than that of Ti^{3+}:sapphire if we use Nd:YAG lasers as a pump source. The maximum available pump energy is twice that of Ti^{3+}:sapphire. Nonetheless, extensive efforts to obtain higher peak power have not yet been made. An output energy of 0.1 mJ was obtained before pulse compression of a CPA system [22]. The main limitation to the peak power that can be obtained using Cr^{4+}:forsterite seems to be the excited-state absorption (ESA) at high-fluence pumping. In the work described in this paper, we found the influence of ESA on the gain obtained experimentally was in good agreement with the result of numerical calculation. We constructed a CPA system based on a regenerative amplifier, and obtained 5.2 GW peak power with a pulse duration of 77 fs. This is the highest peak power ever obtained from a Cr^{4+}:forsterite laser. The results obtained experimentally are in good agreement with the results calculated. An optimum design of the regenerative amplifier is proposed on the basis of the model used in the above-mentioned analysis.

1 Kerr-lens mode-locked oscillator and pulse stretcher

The Kerr-lens mode-locked (KML) oscillator we used was an asthmatically compensated Z-fold cavity [23]. A 2-cm-long Brewster-cut Cr:forsterite crystal was set between concave mirrors with a 10 cm radius of curvature. The crystal was mounted in a heat sink cooled to −15 °C by an antifreeze solution and was pumped by 6 W CW Nd:YAG laser (Spectra-Physics' model 3800) focused by a lens with a focal length of 9 cm. A 1% output coupler was used at one end of the cavity, and a pair of SF6 prisms 17.5 cm apart was inserted in order to compensate the group velocity dispersion in the cavity.

This ocsillator produced approximately 0.3 nJ, 53 fs pulses at a 118 MHz repetition rate. The duration of the pulses was measured by the slow-scan autocorrelation, assuming a sech^2 intensity profile (Fig. 1). The spectral width of the pulses was 50 nm (FWHM) (Spectrum C in Fig. 10), which gave the time–bandwidth product of 0.50.

The pulse duration was stretched from 53 fs to ∼ 50 ps by a conventional stretcher [24] consisting of a grating with a groove density of 600 lines/mm, a lens with a focal length of 700 mm, and two plane mirrors. All the reflective elements, including a grating and mirrors, were coated with gold to make them highly reflective. The incident angle of the grat-

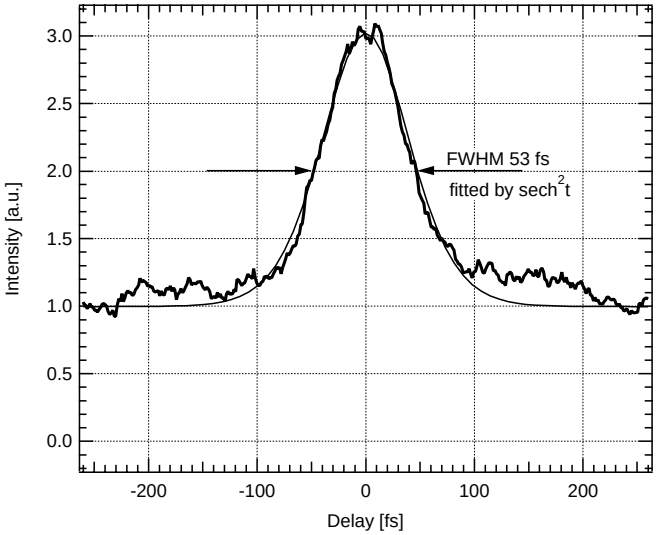

Fig. 1. Autocorrelation trace of Cr:forsterite oscillator

ing was 17.1°, which was 4° apart from the blazed angle at 1270 nm.

2 Small-signal gain measurement of Cr:forsterite

A small-signal gain g_0 is defined in terms of the incident (I_{in}) and transmitted (I_{t}) intensities as

$$I_t = I_{\mathrm{in}} \mathrm{e}^{(g_0-\alpha)L} \tag{1}$$

where L is the crystal length and α is the absorption coefficient.

The intensity transmission of the seed pulses through the crystal, which was pumped by a Q-switched, 10 Hz Nd:YAG laser with the pulse duration of 8 ns, was measured by a fast photodiode. The polarization of the pump beam was oriented along the crystal *b* axis.

The crystal has a dimension of $5 \times 5 \times 5$ mm (the Mitsui Mining and Smelting Company). The total Cr^{4+} ion density (n_0) is 2.1×10^{19} cm^{-3}.

The closed circles in Fig. 2 show the experimentally obtained small-signal gain plotted against pump fluence. The

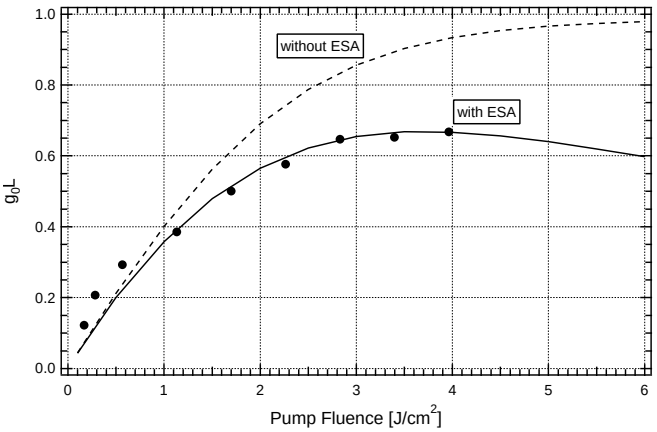

Fig. 2. Gain of Cr:forsterite crystal pumped by a Q-switched Nd:YAG laser. *Closed circles* are experimental results; the *solid* and *broken lines* are calculation results

value of α is estimated to be 0.2 cm^{-1}. The strong saturation evident in Fig. 2 may be due to the depletion of the ground-state and the excited-state absorption. Determing the relative importance of these effects will require a dynamic analysis of the relevant states.

The electronic structures of Cr:forsterite have recently been investigated by absorption and emission spectroscopy. Demos et al. evaluated the photo-excitation process of Cr^{4+} in forsterite by observing upconverted luminescence [25–27]. Figure 3 shows the energy diagram of Cr^{4+} in forsterite [25]. Cr^{4+} is excited from the ground state ($^3A_2$) to the lasing state ($^3T_2$). But the lasing state is also exited, by absorbing 1064-nm light, to ^1E. The state ^1E relaxes to the upper excited state ($^3T_1$), which returns to the lasing state. The ^1E state crosses the $^3T_1$ state, and this crossing produces an electronic bottleneck trap (at 2.1 eV) that delays the nonradiative decay of the excited electron lattice system. The lifetime of the upper excited state is in the order of 10 ps. According to [27], the lifetime of the $^3T_1$ state towards the $^3T_2$ state (lasing state) is in the order of hundreds of ns. The lifetime of the lasing state ($^3T_2$) is well known to be about 2.7 μs.

The rate equations for the transitions shown in Fig. 3 can be written

$$\begin{aligned}
\frac{\partial}{\partial t} n_1 &= -\frac{\sigma}{\hbar\omega_{\mathrm{p}}} I_{\mathrm{p}} n_1 \,, \\
\frac{\partial}{\partial t} n_2 &= \frac{\sigma}{\hbar\omega_{\mathrm{p}}} I_{\mathrm{p}} n_1 - \gamma \frac{\sigma}{\hbar\omega_{\mathrm{p}}} I_{\mathrm{p}} n_2 + \frac{n_3}{\tau} \,, \\
\frac{\partial}{\partial t} n_3 &= \gamma \frac{\sigma}{\hbar\omega_{\mathrm{p}}} I_{\mathrm{p}} n_2 - \frac{n_3}{\tau} \,, \\
\left(\frac{\partial}{\partial z} + \frac{1}{c} \frac{\partial}{\partial t} \right) I_{\mathrm{p}} &= -\sigma (n_1 + \gamma n_2) I_{\mathrm{p}} \,,
\end{aligned} \tag{2}$$

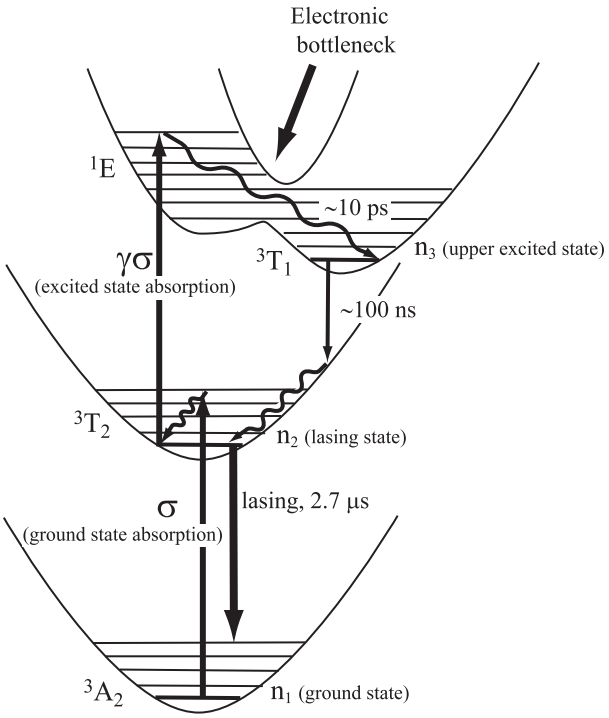

Fig. 3. Energy diagram of Cr^{4+} in forsterite (based on [25])

where n_1, n_2, and n_3 are, respectively, the densities of the ground state ($^3A_2$), the lasing state ($^3T_2$), and the upper excited state ($^3T_1$), and where τ is the lifetime of $^3T_1$. The initial values are $n_1 = n_0$, $n_2 = 0$, and $n_3 = 0$, where n_0 is the total ion density. The transition from ^1E to $^3T_1$ is very fast, so the density of the ^1E state is not taken into consideration. And because the lifetime of the lasing state is much longer than the duration of the pump beam pulses, the spontaneous emission from the $^3T_2$ state can also be neglected. The term I_p is the pump intensity, which is assumed to have a Gaussian temporal profile, ω_p is the frequency of the pump beam, σ is the absorption cross section of the ground state, and $\gamma\sigma$ is the cross section of excited-state absorption. The small-signal gain is given by

$$g_0 L = \sigma_\mathrm{e} \int_0^L n_2 \, \mathrm{d}z \,, \tag{3}$$

with σ_e the laser gain cross section.

The solid line in Fig. 2 shows a numerical calculation of $g_0 L$ with $\sigma_\mathrm{e} = 9.4 \times 10^{-20}\,\mathrm{cm}^2$ [7], $\sigma = 1.9 \times 10^{-19}\,\mathrm{cm}^2$ (which is estimated below), $\gamma = 0.3$ [28], and $\tau = 100\,\mathrm{ns}$. The value of τ is determined from the best fit to the experimental data.

We measured the transmittance of the pump beam through the Cr:forsterite crystal. The transmittance, given by

$$T_\mathrm{e} = \frac{\int \mathrm{d}t \, I_\mathrm{p}(z = L)}{\int \mathrm{d}t \, I_\mathrm{p}(z = 0)} \,, \tag{4}$$

is approximated by $\exp(-\sigma n_0 L)$ when the pumping energy is low. The transmittance versus pump fluence is shown in Fig. 4, where the experimental points are compared with the curve calculated using (4). The absorption cross section σ is estimated to be $1.9 \times 10^{-19}\,\mathrm{cm}^2$ from the transmittance at a zero fluence. The broken line is the transmittance calculated neglecting the ESA (i.e. $\gamma = 0$). When the fluence is low the transmittance calculated with the ESA does not differ much from that calculated without ESA, but the difference increases rapidly with increasing pump fluence.

From (2) the maximum conversion efficiency can be calculated. The maximum conversion efficiency is defined as

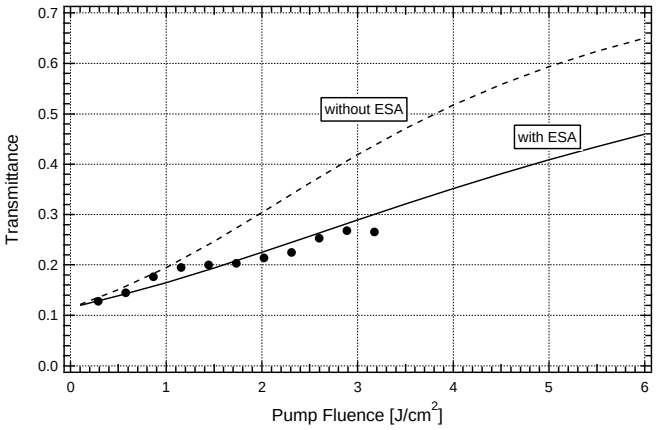

Fig. 4. Transmittance of pump laser. *Closed circles* are experimental results; the *solid* and *broken lines* are calculation results

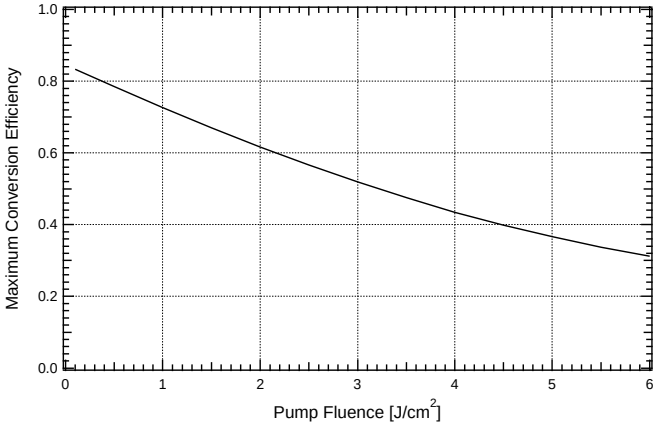

Fig. 5. Calculated maximum conversion efficiency of Cr:forsterite crystal versus pump fluence

$\eta = \varepsilon_\mathrm{sto}/\varepsilon_\mathrm{abs}$, where ε_sto is energy stored in the lasing state, and ε_abs is the energy absorbed by the crystal (per unit cross section). The absorbed energy per unit cross section is written as

$$\varepsilon_\mathrm{abs} = (1 - T_\mathrm{e})\varepsilon_\mathrm{p} \,, \tag{5}$$

where ε_p is the pump fluence given by $\int \mathrm{d}t \, I_\mathrm{p}(z = 0)$. The stored energy per unit cross section is written as

$$\begin{aligned} \varepsilon_\mathrm{sto} &= \hbar\omega \int_0^L \mathrm{d}z \, n_2 \\ &= \frac{\hbar\omega}{\sigma_\mathrm{e}} g_0 L \,, \end{aligned} \tag{6}$$

where $\hbar\omega$ is the photon energy at the laser wavelegth. Figure 5 shows the maximum conversion efficiency versus pump fluence. The maximum conversion efficiency is above 0.8 at low fluence, corresponding to the quantum efficiency (laser wavelength/the pump wavelength). At a pump fluence of $6\,\mathrm{J/cm}^2$, on the other hand, it goes down to 0.3. This shows the fundamental limitation on the power of this kind of amplifier. Furthermore, the gain is not high enough for a multipass amplifier to extract the stored energy efficiently. This analysis shows an efficient high-power laser system cannot be made without using regenerative amplification.

3 High-voltage Pockels cell driver for a regenerative amplifier

At 1270 nm the half-wave voltage of a 99% deuterated potassium dihydrogen phosphate (KD*P) Pockels cell is estimated to be $\approx 10\,\mathrm{kV}$. Even though we operate a regenerative amplifier at a quarter-wave voltage, the voltage is too high for a commercial Pockels cell driver. We therefore developed a high-voltage driver for use in the present experimental work.

Pockels cell drivers used high-speed switches, cold cathode tubes, triggered spark gaps, krytrons, and avalanche transistors [29–32]. We used fast high voltage transistor switches (Behlke Electronic, HTS 50-12-UF) having a very fast rise

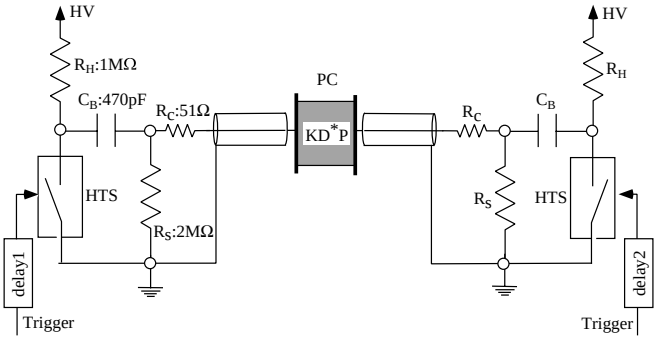

Fig. 6. Fast switching circuit for Pockels cell driving. PC, Pockels cell; HTS, fast high-voltage transistor switch

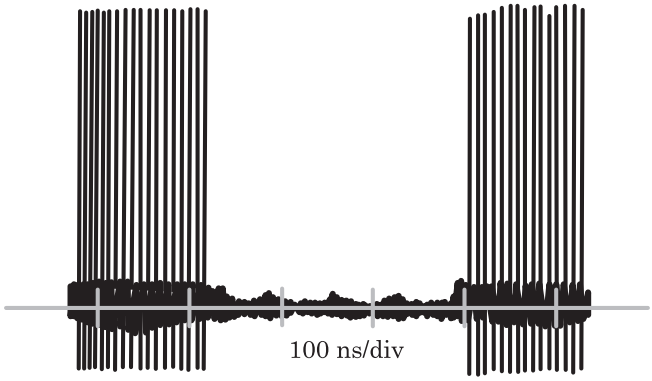

Fig. 8. The pulse train rejected from the regenerative amplifier cavity. The pulse train is introduced into the cavity and cannot be seen from TFP1, applying a high voltage on Pockels cell

time, a high repetition rate, a very low jitter, and a lifetime typical for a semiconductor device. This switch is made of a large number of MOSFETs, parallel and in series, in a compact, low-inductance package. Unlike avalanche transistor switches, the MOSFETs of the HTS switches are not operated in the breakdown mode but are instead controlled by means of their gates. The HTS has a turn-on rise time of 1.6 ns (from the data sheet of HTS).

The driving circuit (Fig. 6) is based on a LC circuit, then the current through HTS is kept low as compared with the circuit with a 50 Ω termination [33, 34]. When the HTS turn on, the charge stored in C_B is transfered rapidly to the capacitor (C_S) of a 25-cm-long coaxial cable (RG59/BU) connected to one side of the Pockels cell. The 51 Ω resistor is inserted in order to suppress the surge voltage and ringing. Because C_B is substantially larger than C_S, a voltage essentially equal to the charging voltage is applied to the electrode of the Pockels cell for the duration of $R_S \times C_S$. This time constant, which is also the recovery time of this circuit, is 50 μs with $R_S = 1\,\mathrm{M\Omega}$ and $C_S = 38\,\mathrm{pF}$. By applying the step voltage on both electrodes of the Pockels cell with a delay time, a rectangular voltage with a pulse duration of a given delay time is applied across the electrodes.

Figure 7 shows the configuration of the regenerative amplifier. The Pockels cell has a KD*P crystal in an index matching liquid and has BK7 windows coated to be antireflective at 1250 nm. The Pockels cell is initially set as a quarter-wave plate by slightly tilting the optical axis of KD*P. By applying a rectangular pulse with a quarter-wave voltage to the Pockels cell, the seed pulse is injected and the amplified pulse is rejected at the rise and fall of the voltage, respectively, through the thin film polarizer. Figure 8 shows the pulse train rejected from the regenerative amplifier. During the application of high voltage on the Pockels cell, the pulses transits back and forth in the cavity and cannot be seen through TFP1. On the other hand, the pulse train is rejected out of the cavity without a high voltage on the Pockels cell. The contrast of the pulse intensity with and without the application of a high voltage shows the extinction ratio of the Pockels cell. The extinction ratio is typically 1:150 at an applied voltage of 5 kV.

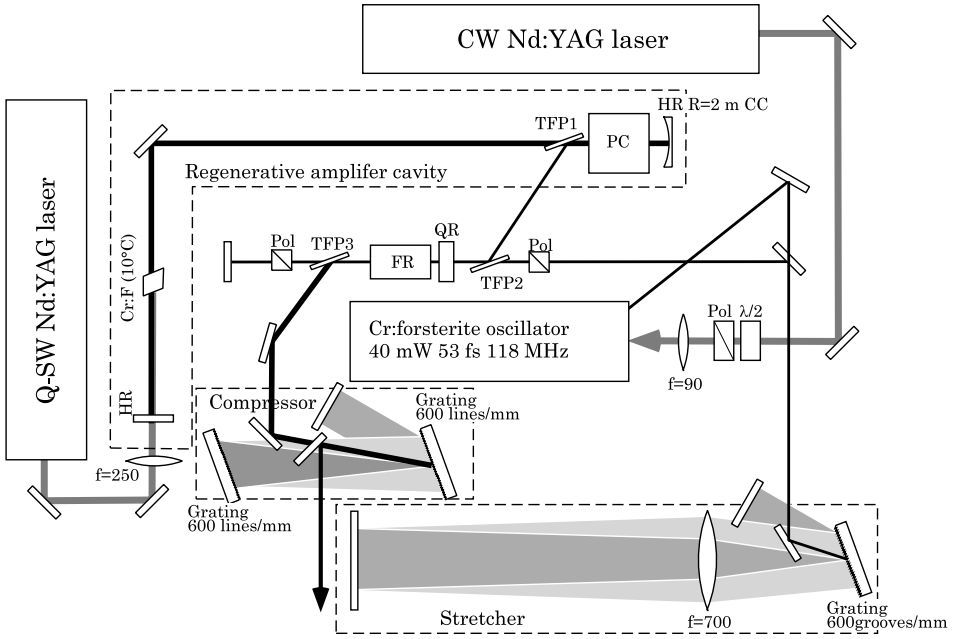

Fig. 7. Schematic diagram of Cr:forsterite laser system consisting of an oscillator, a stretcher, a regenerative amplifer, and a compressor. HR, high reflector; PC, Pockels cell; TFP, thin-film polarizer; FR, Faraday rotator; QR, Quartz rotator; Pol, polarizer; λ/2, half-wave plate

Since the output and the input beams of the amplifier are coaxial, a Faraday rotator (FR) and a quartz rotator (QR) are placed between two thin-film polarizers (TFP2, TFP3) in other to separate them. The Faraday rotator and the quartz rotator also work as an isolator between the oscillator and the regenerative amplifier.

4 Experiment and analysis of regenerative amplifier

Stretched pulses were injected into a 1.5-m-long regenerative amplifier cavity. The cavity consists of a concave mirror (radius of curvature 3 m) and flat mirror. A Brewster-cut Cr:forsterite crystal 5 mm long was kept at 10 °C by a Peltier cooler. A Q-switched, 10 Hz Nd:YAG laser (Spectra-Physics' DCR-11) was used to pump the regenerative amplifier. The crystal was coaxially pumped, at 1064 nm, with 140-mJ 8-ns pulses. A lens with a focal length of 250 mm imaged the pump beam onto the Cr:forsterite crystal at a pump fluence of 3.7 J/cm^2 on the face of the crystal.

Figure 9 shows the evolution of the pulse in the cavity, which is mesurement of the leakage light through the mirror M1 without rejection of the pulse. The first pulse corresponds to the pump beam. The peak of the pulse train appears 250 ns after the injection of the seed pulse. The decay of the pulse train is due to the gain depletion and the loss in the cavity. The highest energy achieved, when the pulse was extracted at 250 ns after injection, was 0.8 mJ. This regenerative amplifier provides a net gain of approximately 10^6 after 25 round trips through the cavity (see Fig. 2).

Figure 10 shows a comparison of the spectra of the output pulse (A), the free-running operation of the regenerative amplifier pumped by a pulsed Nd:YAG laser (B), and the oscillator (C). The spectral width (FWHM) in Spectrum A is 20 nm, and the central wavelengths of Spectrum B and Spectrum C are separated from each other by 50 nm. In the Cr:forsterite crystal, the peak gain is around 1230 nm, but the absorption is lower at longer wavelengths. In the Kerr-lens mode-locked oscillator, which is operated at a low gain, the absorption plays a dominant role in determining the optimum wavelength, resulting in operation at the longer wavelength. On the other hand, in the pulsed oscillator, which is operated by the regenerative amplifier in this experiment, the gain is much larger than absorption, resulting in operation at the shorter wavelength. In regenerative amplification, the spectrum of the amplified pulse is distributed between A and B.

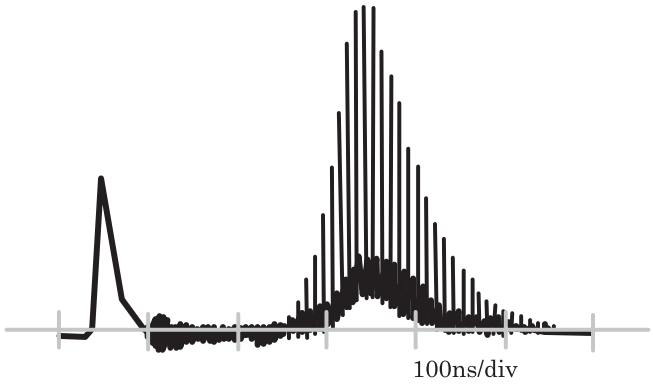

Fig. 9. Pulse evolution in the regenerative amplifier seen from the leakage light through the cavity mirror without rejection of pulses. The first spike corresponds to the pump light

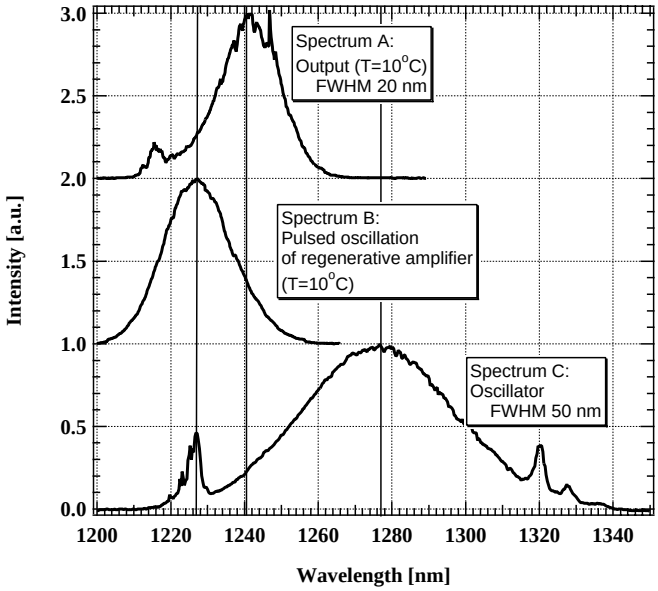

Fig. 10. Spectrum of output pulse (spectrum A), pulsed oscillation of regenerative amplifier (spectrum B), oscillator (spectrum C)

The amplification of a laser pulse can be treated numerically by the addition of absorption to the Franz and Nodvik analysis [35, 36]. It has been reported that Cr:forsterite has absorption by Cr^{2+} at lasing spectrum region [2].

Pulse propagation in the gain medium is can be evaluated by using the following equation:

$$\frac{\mathrm{d}}{\mathrm{d}z}\frac{\varepsilon}{\varepsilon_\mathrm{s}}+\alpha\frac{\varepsilon}{\varepsilon_\mathrm{s}}+g_0\exp(-\frac{\varepsilon}{\varepsilon_\mathrm{s}})=g_0\,, \tag{7}$$

where ε is the laser beam fluence, $\varepsilon_\mathrm{s}=\hbar\omega/\sigma_\mathrm{e}$ is the saturation fluence, g_0 is the gain of the medium, α is the absorption coefficient, and the fluence at $z=0$ is $\varepsilon=\varepsilon_\mathrm{in}$.

The solution of (7) can be defined as the function of z, ε_in, g_0, and α as the following:

$$\frac{\varepsilon}{\varepsilon_\mathrm{s}}=f(z,\varepsilon_\mathrm{in},g_0,\alpha)\,. \tag{8}$$

Therefore the output fluence passed through the gain medium with a length of L, ε_out, is given by

$$\frac{\varepsilon_\mathrm{out}}{\varepsilon_\mathrm{s}}=f(L,\varepsilon_\mathrm{in},g_0,\alpha)\,. \tag{9}$$

For many round trips in the cavity, we use the recursive relation for the round trip number k [37]. At the k round trip,

$$\frac{\varepsilon_\mathrm{out}^{(k)}}{\varepsilon_\mathrm{s}}=f(2L,\varepsilon_\mathrm{in}^{(k)},g_0^{(k)},\alpha)\,. \tag{10}$$

α is constant, and $g_0^{(k)}$ decreases each passing of the pulse. Therefore $g_0^{(k)}$ is given by

$$g_0^{(k)}=g_0^{(k-1)}-\frac{\varepsilon_\mathrm{out}^{(k-1)}-\varepsilon_\mathrm{in}^{(k-1)}}{\varepsilon_\mathrm{s}L}\,. \tag{11}$$

Losses due to reflection, intracavity scattering are introduced by

$$\varepsilon_{\text{in}}^{(k+1)} = (1-R)\varepsilon_{\text{out}}^{(k)} , \tag{12}$$

where R is the round-trip loss.

The closed circles in Fig. 11 show the calculation, where $\varepsilon_{\text{s}} = 1.6\,\text{J/cm}^2$ ($\sigma_{\text{e}} = 9.4\times10^{-20}\,\text{cm}^2$), $g_0^{(0)} = 1.3\,\text{cm}^{-1}$, and $\varepsilon_{\text{in}}^{(0)} = 3\times10^{-9}\,\text{J/cm}^2$. The fitting to the experimental data in Fig. 9 was done with parameters of α and R. The value of α is roughly estimated, from the figure of merit (FOM) of 23 reported in [7], to be $\alpha = 0.2\,\text{cm}^{-1}$. When $\alpha = 0.20\,\text{cm}^{-1}$, $R = 0.20$ this simulation fits for Fig. 11 best.

The fluence can be derived automatically from the fitting. The maximum fluence of $0.4\,\text{J/cm}^2$ in the cavity is in good agreement with the 0.83 mJ output energy when the spot size of 1.2 mm, the reflectance of TFP (80%) and the throughput of FR, QR, and Pol (80%) are taken into account. The open circles in Fig. 11 show the evolution of the pulse train without absorption ($\alpha = 0$). That means the absorption is still serious even in amplification where the gain is much larger than absorption.

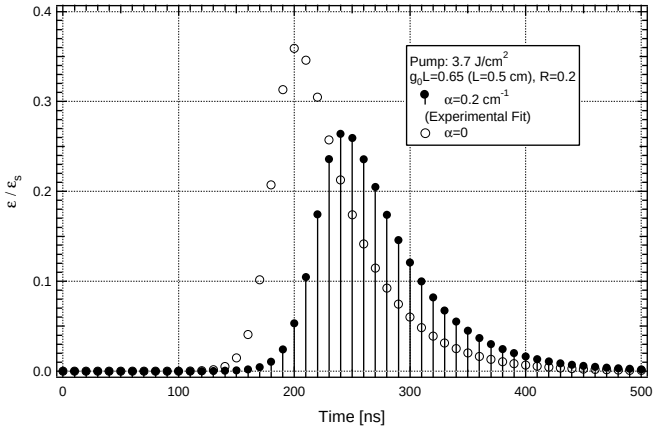

Fig. 11. Simulated pulse evolution. The *closed circles* are the fit to the experimental results (Fig. 9), and the *open circles* are without absorption. The vertical axis is the fluence normalized by the saturation fluence ε_{s}

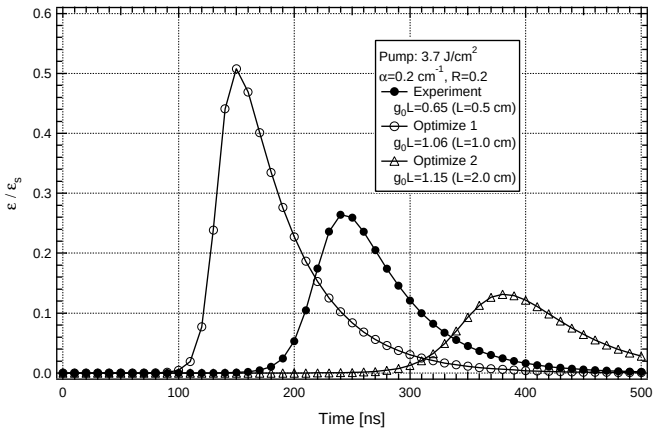

Fig. 12. Simulated pulse evolution with crystal lengths of 0.5 cm, 1.0 cm, and 2.0 cm. The vertical axis is the fluence normalized by the saturation fluence ε_{s}

Based on the simulation, the direction to the optimization can be shown. We know from the results shown in Fig. 4 that the transmittance of the pump beam is 30% when the crystal is 0.5 cm long. Increasing the length L of the crystal increases the absorbed energy and results in a higher $g_0 L$. At a pump fluence of $3.7\,\text{J/cm}^2$, the values of $g_0 L$ are 0.65 for $L = 0.5$ cm, 1.06 for $L = 1$ cm, and 1.15 for $L = 2$ cm. The value of αL, however, increase linearly with increasing the crystal length. The simulated pulse evolution is shown for various crystal lengths in Fig. 12. The fluence with $L = 1$ cm is larger by a factor of 1.7 than that with $L = 0.5$ cm. With $L = 2$ cm, however, the fluence is half of that with $L = 0.5$ cm.

5 Pulse compression

The amplified pulses are compressed by the double pass through a grating pair. This grating has a groove density of 600 lines/mm. The compressor was adjusted to minimize the pulse duration, and this was done by taking into account the spectral shift of the amplified pulse and the dispersion of materials. As a result, the incident angle was 17° and the center-to-center distance between gratings was 70 cm.

A single-shot autocorrelation was used to measure the pulse duration, and a typical autocorrelation trace of the compressed pulse is shown in Fig. 13, As the result, the pulse duration is 77 fs, assuming a sech^2 intensity profile. The bandwidth of the output pulse is 20 nm, and this means that the time–bandwidth product is 0.30. This value suggests the compressed pulse is almost transform limited. The measured energy of the compressed pulse was 0.4 mJ, which implies a peak power of 5.2 GW. The throughput of the compressor is therefore about 50%.

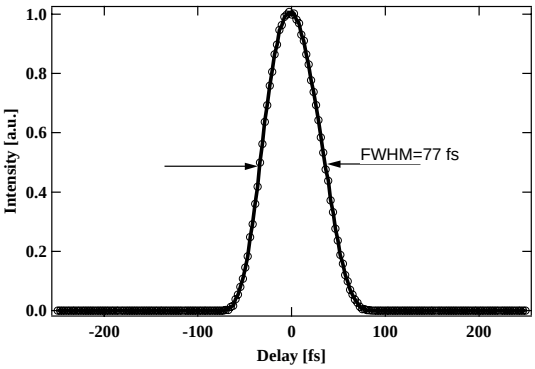

Fig. 13. Single-shot autocorrelation trace of the compressed pulse

6 Conclusion

We have developed a high-power Cr:forsterite laser system by using a regenerative amplifier. The output energy at 1240 nm was 0.4 mJ when the pulse duration was 77 fs. This resulted in a peak power of 5.2 GW, which as far as we know is the highest power ever obtained from a Cr:forsterite laser. To make this system, we developed a high-voltage Pockels cell driver based on fast, high-voltage transistor switches. The influence of the excited-state absorption on gain was investigated experimentally and numerically, and the experimentally

obtained results are in good agreement with the calculated results. The simulation results obtained taking into account an absorption in the crystal as well as excited-state absorption show how the output of this laser system can be optimized.

References

1. V. Petričević, S.K. Gayen, R.R. Alfano, K. Yamagishi, H. Anzai, Y. Yamaguchi: Appl. Phys. Lett. **52**, 1040 (1988)
2. V. Petričević, S.K. Gayen, R.R. Alfano: Appl. Phys. Lett. **53**, 2590 (1988)
3. H.R. Verdun, L.M. Thomas, D.M. Andrauskas, T. McCollum: Appl. Phys. Lett. **53**, 2593 (1988)
4. V. Petričević, S.K. Gayen, R.R. Alfano: Opt. Lett. **14**, 612 (1989)
5. T.J. Carrig, C.R. Pollock: Opt. Lett. **16**, 1662 (1991)
6. G. Onishchukov, W. Hodel, H.P. Weber: Opt. Commun. **100**, 137 (1993)
7. I.T. McKinnie, L.A.W. Gloster, Z.X. Jiang, T.A. King: Appl. Opt. **35**, 4159 (1996)
8. I.T. McKinnie, L.A.W. Gloster, Z.X. Jiang, T.A. King: Opt. Commun. **129**, 49 (1996)
9. T. Fujii, M. Nagano, K. Nemoto: IEEE J. Quantum Electron. **QE-32**, 1497 (1996)
10. A. Seas, V. Petričević, R.R. Alfano: Opt. Lett. **17**, 937 (1992)
11. A. Seas, V. Petričević, R.R. Alfano: Opt. Lett. **18**, 891 (1993)
12. Y. Pang, V. Yanosky, F. Wise: Opt. Lett. **18**, 1168 (1993)
13. Z. Zhang, K. Torizuka, T. Itatani, K. Kobayashi, T. Sugaya, T. Nakagawa: IEEE J. Quantum Electron **QE-33**, 1975 (1997)
14. A. Sennaroglu, C.R. Pollock, H. Nathel: IEEE J. Quantum Electron **QE-30**, 1851 (1994)
15. I.T. McKinnie, A.L. Oien: Opt. Commun. **141**, 157 (1997)
16. A. Baltuska, Z. Wei, M.S. Pshenichnikov, D.A. Wiersma: Opt. Lett. **22**, 102 (1997)
17. M. Nisoli, S.D. Silveatri, R. Szipocs, C. Spielmann, S. Sartania, F. Krausy, K. Ferency, O. Svelto: Opt. Lett. **22**, 522 (1997)
18. S. Backus, C.G. Durfee III, G. Mourou, H.C. Kapteyn, M.M. Murnane: Opt. Lett. **22**, 1256 (1997)
19. J.P. Chambaret, C.L. Blanc, G. Chériaux, P. Curley, G. Darpentigny, P. Rousseau, G. Hamoniaux, A. Antonetti, F. Salin: Opt. Lett. **21**, 1921 (1996)
20. J. Itatani, Y. Nabekawa, K. Kondo, S. Watanabe: Opt. Commun. **134**, 134 (1997)
21. D. Strickland, G. Mourou: Opt. Commum. **56**, 219 (1985)
22. J.M. Evans, V. Petricevic, A. Delgrado, R.R. Alfano: CLEO'96.Summaries of Papers Presented at the Conference on Laser and Electro-optics **9**, 127 (1996)
23. G.R. Boyer, G. Kononovitvh: Opt. Commun. **133**, 205 (1997)
24. J. Squier, G. Korm, G. Mourou: Opt. Lett. **18**, 625 (1993)
25. S.G. Demos, R.R. Alfano: Phys. Rev. B **46**, 8811 (1992)
26. S.G. Demos, Y. Takiguchi, R.R. Alfano: Opt. Lett. **18**, 522 (1993)
27. S.G. Demos, V. Petrićevič, R.R. Alfano: Phys. Rev. B **52**, 1544 (1995)
28. H.R. Verdún, L. Merkle: OSA Proceedings on Advanced Solid-State Lasers, 1991, Vol. 10
29. I. Matsushima, T. Kasai, M. Yano: Rev. Sci. Instrum. **52**, 1860 (1981)
30. J.M. Ley, T.M. Christmas, C.G. Wildey: Proc. IEEE **117**, 1057 (1970)
31. R.C. Myer, H.D. Sutphin, K.R. Winn: Rev. Sci. Instrum. **46**, 1333 (1975)
32. S.J. Davis, J.E. Murray, D.C. Downs, W.H. Lowdermilk: Appl. Opt. **17**, 3184 (1978)
33. P. Bado, M. Bouvier: Rev. Sci. Instrum. **56**, 1744 (1985)
34. K. Becker, J.B. Johnson, G. Edwards: Rev. Sci. Instrum. **65**, 1496 (1994)
35. L.M. Frantz, J.S. Nodvik: J. Appl. Phys. **34**, 2346 (1963)
36. M.M. Tilleman, J.H. Jacob: Appl. Phys. Lett. **50**, 121 (1987)
37. F.P. Strohkendl, D.J. Files, L.R. Dalton: J. Opt. Soc. Am. B **11**, 742 (1994)